Analysis of Cu-wire pull and shear test failure modes under ageing cycles and finite element modelling of Si-crack propagation

S. Mazzei [a], M. Madia [b,*], S. Beretta [a], A. Mancaleoni [c], S. Aparo [c]

[a] *Politecnico di Milano – Mechanical Department, Italy*
[b] *BAM – Federal Institute for Materials Research and Testing, Division 9.1, Berlin, Germany*
[c] *ST-Microelectronics Automotive Product Group – Testing and Reliability Engineering, Agrate Site, Italy*

Article history:
Received 22 July 2013
Received in revised form 2 April 2014
Accepted 3 April 2014
Available online 10 May 2014

1. Introduction

In microelectronic packaging, wire bonding is the predominant method for making electrical connections between the silicon chip and the package lead-frame. Gold wire is the most popular interconnection material used in the wire bonding process. However, gold is increasingly substituted by copper since copper is not only a much cheaper alternative but it also offers several physical advantages such as better mechanical, electrical and thermal properties [1,2]. On the other hand, since copper is stiffer than gold, the window available for the optimization of wire bonding process parameters is much narrower [3,4]: higher bonding force and ultra-sonic energy are necessary to create a reliable connection to the silicon chip I/O pads, with a reduced margin against damaging their multi-layer structure, consisting of alternate metal and dielectric thin films.

These constraints represent the main task for wire-bonding process optimization on smart-power ICs, where high current capability and low output resistance requirements can strictly be met through the adoption of thick bonding wires (from 1.2 mil up to 3 mil gold, being replaced by 1.2 mil up to 2.5 mil pure copper). This is the main scope of the present paper, which deals with silicon and packaging technologies commonly used for medium-power integrated circuits.

The results here described are not directly applicable to advanced fine-pitch CMOS ICs with complex bond-pad stack and low-k dielectrics. These are usually bonded with small diameter copper (less than 1 mil), and the primary concern is the wire workability at 1st and 2nd bond tips; this has been effectively addressed through the use of Pd-coated copper wire, which mitigates the risk of wire and free-air ball oxidation.

For smart-power components, often exposed to harsh application environments, the risk that micro-damages induced during the wire-bonding process could evolve into more severe cracks during the component field life often obliges silicon designers to

* Corresponding author. Tel.: +49 (0) 30 8104 4166; fax: +49 (0) 30 8104 1539.
E-mail address: mauro.madia@bam.de (M. Madia).

Nomenclature

d	distance in Fig. 1
r	radial coordinate about the crack tip
AF	acceleration factors
E	elastic modulus
FEM	finite element method
FIB	focused ion beam
FM	failure mode
F	applied force
F_{wd}	force acting on the ball bond
F_{wt}	force acting on the stitch bond
G	shear modulus
h	distance in Fig. 1
H	distance in Fig. 1
HTS	high temperature storage
IMC	intermetallic compound
K_1, K_2	complex stress intensity factors
K_I, K_{II}	standard mode stress intensity factors
PMC	post mold curing
SEM	Scanning Electron Microscope
SIF	stress intensity factor
TC	Temperature Cycles
α, β	Dundurs parameters
ε	parameter in Fig. 1
ϕ	angle in Fig. 1
θ	angular coordinate about the crack tip
θ_0	crack propagation direction
ν	Poisson's ratio
σ	standard deviation
σ_θ	hoop stress about the crack tip
Δa	crack extension
ΔF	difference in mechanical strength
ΔSIF	difference in stress intensity factor

avoid active circuits and metal routing under the bond-pad area. But also in case of purely "passive" bond-pads (i.e. all metal levels shorted and no active areas below), the maximum tolerable level of micro-damages induced by copper bonding has to be accurately characterized and controlled during massive manufacturing, in order to assure an adequate and reliable mechanical integrity of the connection.

The commonly-used process controls for the mechanical reliability of wire-bonding are the "wire pull" and the "ball bond shear" tests [5–7]. During process validation they are assumed as a key indicator for the process optimization (DOE) and often repeated on reliability-aged samples, even in absence of functional failures, in order to assess the lifetime margins. One of the most alarming failure modes in wire pull and ball shear testing is the so-called "cratering" whereby the silicon substrate under the ball bond breaks before the copper wire itself (pull) or the top metal interface (shear) [8]. This could reflect an undesired weakening of the bond-pad structure due to excessive bonding force and energy, or represent a possible intrinsic breaking mode for the system when submitted to the test, neither activated by pre-existing defects nor by reliability stresses, and not therefore to be assumed as a symptom of functional failure risk during the component field life.

Mechanical cross-sections of the bonds pulled or sheared in correspondence of different step of stress have been used as a way to investigate how the failure modes are generated and propagated in the bond-pad structure during the destructive testing. Corner conditions of the wire-bonding parameters intentionally set at the upper limit of the process window, and accelerated stress treatments close to simulate the most severe reliability requirements, have been implemented on the test samples in order to explore the most critical area for pull and shear test responses. This approach reflects a recommended practice in reliability testing in a perspective of "robustness improvement".

Moreover, a finite element model has been developed in order to simulate pull and shear tests. In this way, an efficient and reliable tool is provided to predict the bond behaviour and possible problems concerning its interface deterioration rate through the usage of the stress intensity factor (SIF) from the linear elastic fracture mechanic [9].

The potentiality of a numerical approach in the failure prevision and study is utterly interesting: not only for being faster and cheaper than an experimental campaign but, especially, for being able to simulate many different situation and explore various scenarios simultaneously in order to understand the significant variables of the problem.

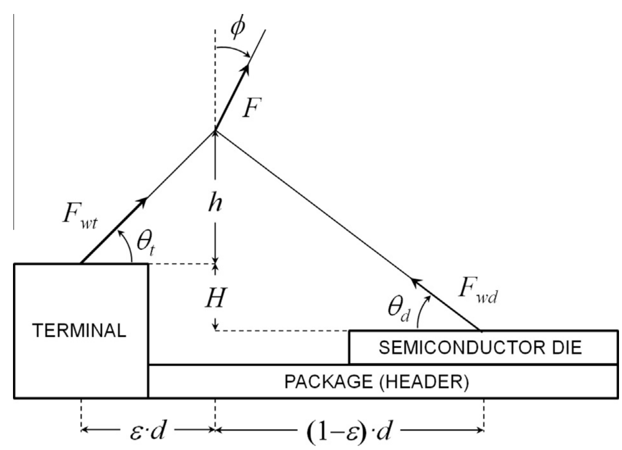

Fig. 1. Outline of pull test geometry [7].

Finally, the innovation concerning the use of the SIF as a characterizing parameter, presented in this article, can be fundamental to develop a further aspect useful for the prevision of interface reliability and deterioration: acceleration factors (AF) are often based on Coffin–Manson law [10], but this law is not applicable to materials in presence of damages or cracks; a new AF based on the SIF is being developed. This new AF can be suitable for predicting the bond reliability under different conditions.

2. Experimental

In order to investigate the wire pull and ball shear test failure modes, two different batches of a same device have been submitted to accelerated stress treatments [11]. A total amount of 56 units has been tested through wire pull test [12,13] and ball shear test [14,15], containing 1120 copper wire bonds.

A smart-power device has been used to build the test samples, in which the bond-pad structure consists of a 3.1 μm-thick AlSiCu film sputtered over a silicon area free of active components. A 2.7 μm-thick silicon oxide stack insulates the bond-pad metal plate from the silicon. The device is assembled in a power surface mounting package encapsulated by halogen-free mold compound. Pure copper wire (4 N type) has been used to connect the bond-pads to the package lead-frame, offering adequate electrical conductivity to meet the R_{DSON} targets for the selected device.

A thermo-sonic wire bonding process has been adopted. Thanks to the high melting point of the die-attach material, based on PbSnAg soft-solder, the bonding temperature could be set at 240 °C. A forming gas flow around the bonding tool prevented FAB (Free Air Ball) oxidation during the bonding phase.

The first batch of units has been assembled with a 2 mil copper wire, using the nominal wire bonding process parameters from a previous DOE; the target bonded ball diameter and height were 140 μm and 35 μm, respectively. The second batch has been assembled with a 2.5 mil wire using the "upper corner" parameters (maximum bonding force and ultra-sonic power) determined for a bonded ball diameter of 150 μm, keeping the same ball height as for the 2 mil batch.

In terms of bond force and ultrasonic power per area unit, the second batch required a 40% increase of these two inputs parameters with respect to the first batch. Accordingly, the second batch was expected to exhibit a more severe compression of the AlSiCu metal compared to the first batch, with increased probability that micro-defects are induced at the underlying dielectric interface. Polished cross sections have confirmed a good interface flatness on the 2 mil ball bonds, with 1 μm of residual AlSiCu below the CuAl intermetallic phases, while the 2.5 mil ball bonds exhibited a remarkable deformation at their interface with the underlying metal, leaving a residual AlSiCu thickness often lower than 1 μm in the bond peripheral region.

The main purpose of the second batch was to compare pull and shear test responses, and then model the related failure modalities, in a borderline situation for the mechanical impact of the ball bonding operation, approaching the maximum tolerable stress for the bond-pad structure integrity. From this perspective, it is important to remark that both the recipes used to generate the samples batches came from a DOE procedure which included the absence of evident oxide or silicon damage (cratering) among the optimization targets. This is normally verified through a "cratering test" method consisting of ball bond and bond-pad metal chemical etch, followed by an optical inspection of the exposed dielectrics at 10× to 50× magnification. So the tested samples were reasonably free of pre-existing oxide or silicon cracks inside the bonding area induced during the wire bonding operation.

For each batch, four sample groups have been thus analysed as shown in Table 1 corresponding to stress situations described in Table 2:

Un-molded: units did not experience any additional assembly operation or ageing treatment after the thermo-sonic wire bonding. This sample represents the time-0 reference without any ageing; the physical condition of the bonds is that determined by the wire-bonding operation itself. In-process statistical controls for the wire-bonding step are usually performed at this stage.

Molded: units were taken out of the plastic molding and Post-Mold Curing (PMC) operations, which impose a 4–10 h isothermal bake at 175 °C, typically. This is representative of the ageing level resulting from the plastic package assembly cycle, as no significant thermal stress is then experienced by the components during the subsequent operations until finishing and functional test.

TC: a number of 500 Temperature Cycles were performed in an air-to-air shock chamber, in the range −65/150 °C with a 15 min dwell time at each temperature (2 cycles/h). This is a standard reliability test [5] simulating both the ON/OFF cycles and the passive temperature swings driven from the external ambient during the component field service.

HTS + TC: a stress sequence consisting of 168 h isothermal storage at 150 °C followed by 500 TC (stress conditions as above) has been implemented, for a more complete simulation of the field application environment, where steady-state operation at high temperature is experienced by the component in parallel to the active and passive temperature excursions.

The possible failure modes from destructive wire pull and ball shear tests are presented in Tables 3a and b, and they can be divided into "acceptable" and "not acceptable" (i.e. potentially critical) on the basis of the consolidated process control practices extensively applied for gold wire-bonding. Broadly speaking, a not acceptable failure mode is a failure mode that highlights a potentially dangerous degradation mechanism for the device reliability, and should therefore trigger a deeper and careful assessment. It is important to underline that the numbering of the failure modes in Table 3 does not fulfil progressive numbering criteria, but the failure modes have been labelled according to internal classification system.

Destructive wire pull test and ball shear data were collected in correspondence of the four different stress situations for the two batches of units. Two different aspects of each test have been recorded: the occurrence frequency of each failure mode (in percent) and the correspondent mean breaking force (in grams). A "DAGE BT 4000" bond tester has been used, which can accommodate either pull or shear load cartridges with appropriate load ranges and offers the possibility to plot the applied load against test time. Pull and shear test parameters have been optimized, carrying out specific assessments in advance to the data collection.

Pull test has been outlined as shown in Fig. 1 in order to optimize the pulling hook position and minimize the variance in the test results. The force F applied to the hook can be related to the actual forces acting on the ball bond F_{wd} and on the stitch bond F_{wt} through Eqs. (1) and (2) respectively.

$$F_{wd} = F \cdot \left[\frac{\sqrt{1 + \frac{(1-\varepsilon)^2 \cdot d^2}{(h+H)^2}} \cdot (h+H) \cdot \left(\varepsilon \cdot \cos\phi - \frac{h}{d} \cdot \sin\phi\right)}{h + \varepsilon \cdot H} \right] \tag{1}$$

$$F_{wt} = F \cdot \left[\frac{\sqrt{h^2 + \varepsilon^2 \cdot d^2} \cdot \left((1-\varepsilon) \cdot \cos\phi - \frac{(h+H)}{d} \cdot \sin\phi\right)}{h + \varepsilon \cdot H} \right] \tag{2}$$

Table 2
Stress sources: link between stress treatments and manufacturing or use conditions.

Sample group	Thermo-sonic wire bonding	Plastic package assembly cycle	Thermo-mechanical fatigue	Thermal-aging
Un-molded	✓			
Molded	✓	✓		
TC	✓	✓	✓	
HTS + TC	✓	✓	✓	✓

Table 1
Stress matrix: accelerate stress treatments to which the devices have been submitted.

Sample group	Stress condition	Corresponding moment in device lifetime
Un-molded	–	"Time-0"
Molded	8 h @ 175 °C	Assembled device
TC	500 thermal cycles in the interval −65/+150 °C	ON/OFF cycles and passive temperature swings
HTS + TC	168 h @ 150 °C and subsequent 500 thermal cycles in the interval −65/+150 °C	Complete simulation of the device life in the real environment

Table 3
Failure modes for (a) wire pull test and (b) ball shear test: different possible failure modes with useful abbreviations and identification tags.

Failure mode	Acceptable or not	Label	Tag
(a)			
Wire breakage	Acceptable	FM 2-3	
Ball lift	Not acceptable	FM 1	
Pad lift	Not acceptable	FM 9	
Cratering	Not acceptable	FM 0	

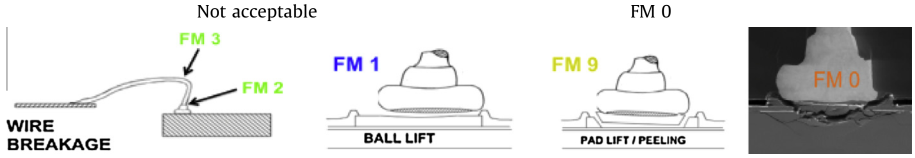

Description	Acceptable or not	Label	Tag
(b)			
Pad shear	Acceptable	FM 1	
Pad lift	Not acceptable	FM 9	
Cratering	Not acceptable	FM 0	

Based on the wire loop geometry of the samples under test, it has been determined that a hook placement close to the ball bond neck, i.e. with $\varepsilon \geqslant 0.95$, and in a vertical position, i.e. $\phi \approx 0°$, reasonably assure that the whole force applied to the hook will act on the ball bond. In particular, it has been found that $F_{wd} \geqslant 0.96$ F. The pulling force has been thus assumed as applied to the ball bond in vertical direction.

Shear test has been performed with the shear tool moving in the same direction as the ultrasonic vibration during the bonding phase, and at a constant height of 4 μm over the chip surface. A higher positioning of the tool has been found to have negligible influence on the test results, while a lower one was not considered due to the presence of passivation steps at the edge of the 3.1 μm-tick metal patterns.

Moreover, cross-sections have been executed, either by mechanical polishing on a "Struers Planapol-V" lapping system, or by Focused Ion-Beam (FIB) techniques on a "Zeiss NVISION 40 cross-beam" equipment, in order to characterize and classify more in detail the differences between the various failure modes and investigate the fracture propagation mechanism. The sectioned units have been observed through the Scanning Electron Microscope (SEM) integrated in the FIB system.

Finally, wire pull and ball shear tests have been repeated in a non-destructive modality in order to identify the critical point of the system: the sense of a non-destructive test is to stop the breakage process at its beginning, so that the crack starting point can be observed and studied. This goal can be achieved only if the load curves related to the destructive and non-destructive modality overlap each other.

Based on preliminary trials, pull test speed was set at the machine default value of 100 μm/s, highlighting a good overlapping between the aforesaid load curves. Shear test speed required a deeper characterization, since the load curves obtained with the machine default value of 100 μm/s led to unsatisfactory results, as shown in Fig. 2a. It was finally possible to select a shear speed of 10 μm/s, with a good compromise between test duration and load curves overlapping, as shown in Fig. 2b.

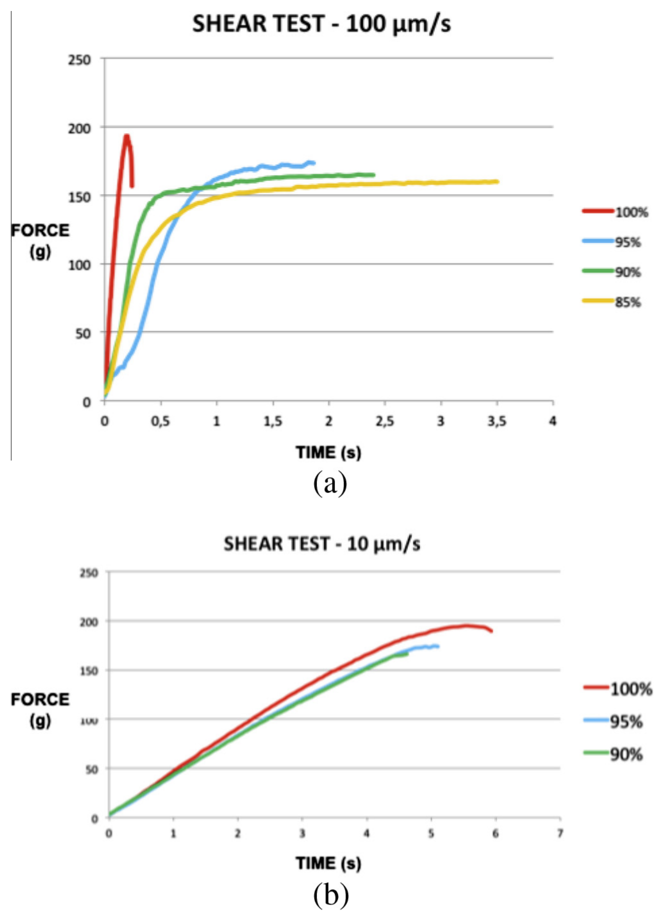

Fig. 2. Shear test load curves obtained for a tool advancing speed of 100 μm/s (a) and 10 μm/s (b) to compare destructive and non-destructive shear tests. Destructive shear test load curves are named 100%. Non-destructive tests have been stopped at a certain percentage of the average braking load detected during the destructive tests and so the relative load curves are named with the corresponding percentage used, i.e. 95%, 90% and 85%.

3. Experimental results

The reliability tests executed on the two batches pointed out a remarkable difference in wire pull and ball shear results, creating a clear scene for the problem characterization. The 2.0-mil batch did not disclose not-acceptable failure modes: all the wires failed at the loop centre or ball neck during pull test, with breaking loads

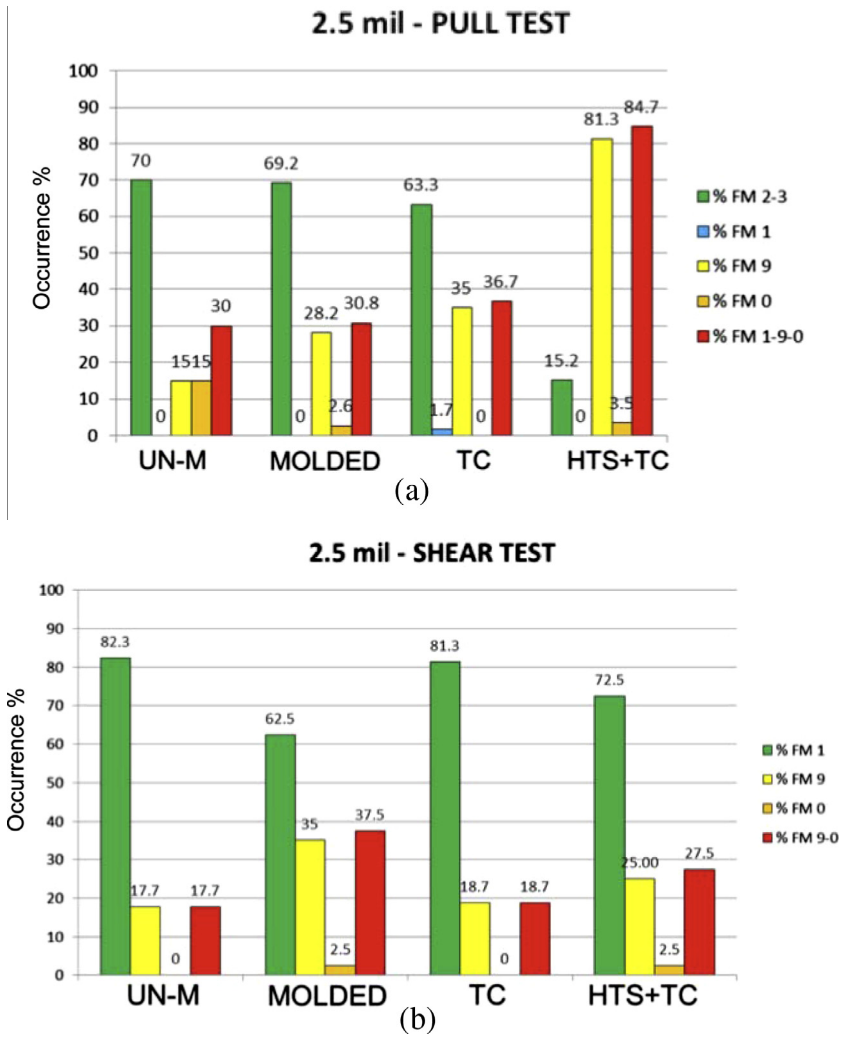

Fig. 3. Occurrence frequency for each failure mode during (a) pull test and (b) shear test of 2.5-mil devices. The last column of each group clusters all the non-acceptable failure modes. Data are presented in increasing order of stress condition.

in the range 44–47 g. The 2.5-mil batch exhibited a significant number of peeling and cratering events even at "time zero". The occurrence frequency for each failure mode during pull test and shear test are presented in Fig. 3a and b, respectively, while the correspondent mean force is shown in Fig. 4a and b.

Pull test can be assumed as a more sensitive tool to detect mechanical weakness and cumulated damage in the ball bonds rather than shear test, either during lot acceptance test at the production line or after reliability trials, for two main reasons:

- The percentage of non-acceptable failure modes during pull test grows with the increased severity of the stress condition (see Fig. 3a) while during shear test it remains almost constant (see Fig. 3b).
- The difference in breaking loads between the acceptable and non-acceptable failure modes is much higher in pull test than in shear test (compare the "distance" between the curves relative to acceptable and not acceptable failure modes in Fig. 4a and b).

Mechanical cross sections of failed bonds show that bonds belonging to the lower tail of the breaking load distribution plot in Fig. 5a show the aluminium pad fractured down to the dielectric surface, with even small and superficial damage of silicon, as shown in Fig. 5b. This highlighted that the deeper the aluminium pad fracture the lower the correspondent breaking force.

A number of pictures and measurements have been taken to analyze the crack propagation at each test condition and compare them with each other. As they all show the same mode of fracture and similar crack propagation direction, figures and values reported in this paper are significant examples representing these common trends.

Non-destructive tests, stopped at the 90% of the average breaking load detected during the destructive tests, have shown cracks to start from the point where the aluminium sliding is just above the dielectric surface. Aluminium sliding has been highlighted in the upper part of Fig. 6 where the sliding path is clearly visible. This point is naturally located in correspondence of the pad "greatly-deformed zone", i.e. that part of the pad characterized by the highest reduction of the AlSiCu metal thickness due to the bonding tool pressure (it corresponds to the edge circumference of the bonding capillary). When the pad top metal plate slides closer to the silicon oxide surface, any defect of the surface finish or surface micro-damages due to the wire-bonding process are expected to intensify the local stress, facilitating the fracture propagation though the silicon oxide and, sometimes, the silicon substrate (see Fig. 6). Moreover, cracking direction, shear tool testing direction and cross section direction, in all condition,

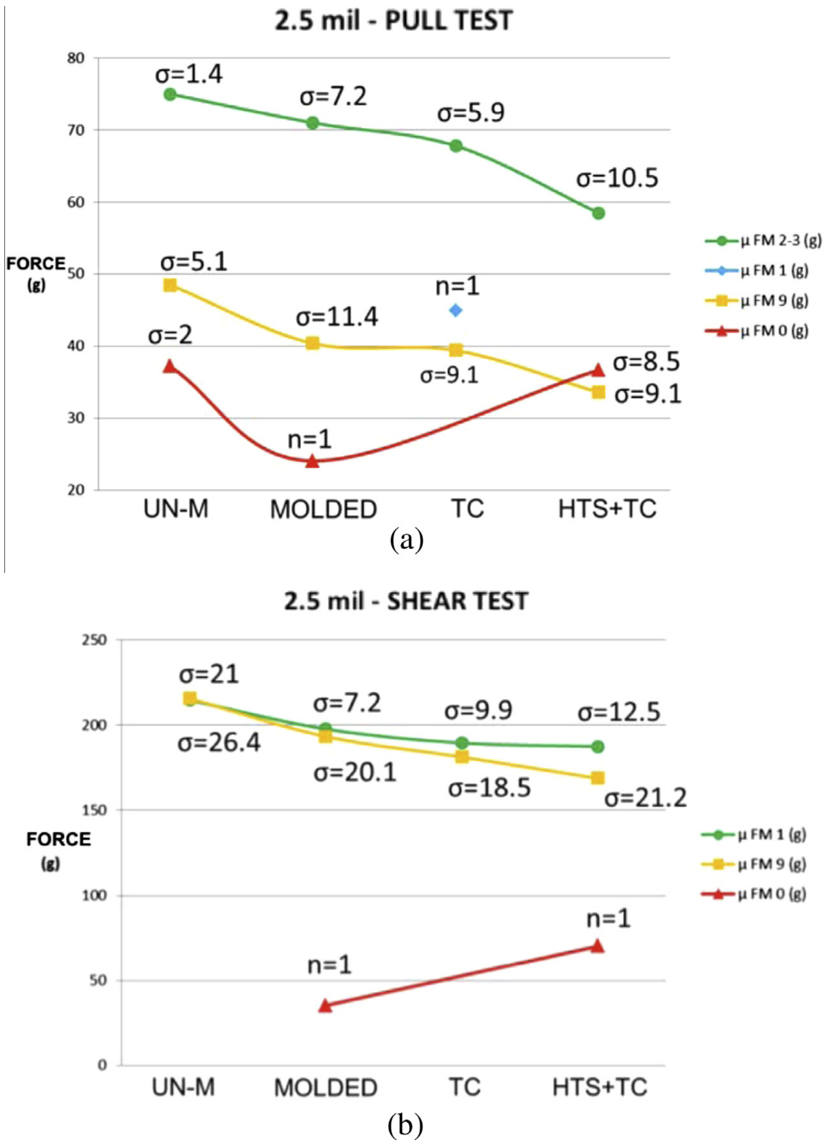

Fig. 4. Mean force for each failure mode occurred during the (a) pull test and (b) shear test. With σ the standard deviation is specified. Data are presented in increasing order of stress condition. For each stress situation, 60 wires have been tested.

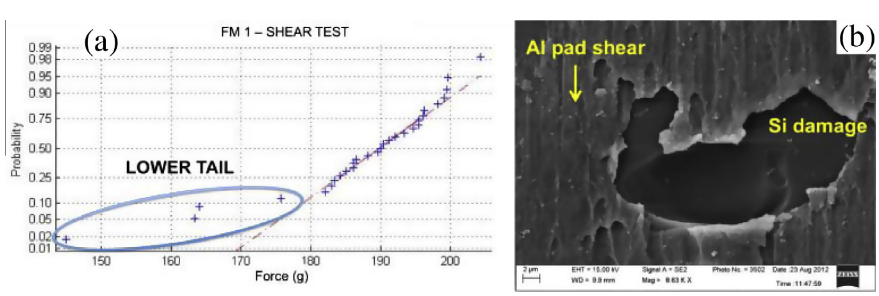

Fig. 5. Bond breaking force probability plot (a) and detail of a failed pad from the lower tail of the graph (b).

has always been the same as ultrasonic direction during bonding, as shown in Fig. 6.

But even in absence of defects at the interface, a high bond-pad metal deformation with residual Al metal minimum thickness lower than 1 μm appears closely correlated with an increased occurrence of not acceptable failure modes during pull and shear tests. Comparing untested bonds cross sections (see Fig. 7), it can be seen that the 2 mil-diameter devices batch, found to be almost free of not acceptable failure modes, exhibits a flatter bond-pad metal all along the ball bond interface. On the other hand, 2.5 mil-diameter devices batch, found to be significantly affected by not acceptable failure modes, exhibits highly deformed zones at the bond interface.

The most critical situation for crack propagation arises when the bond-pad is so greatly deformed that the copper ball bond bottom interface has direct contact points with the underlying

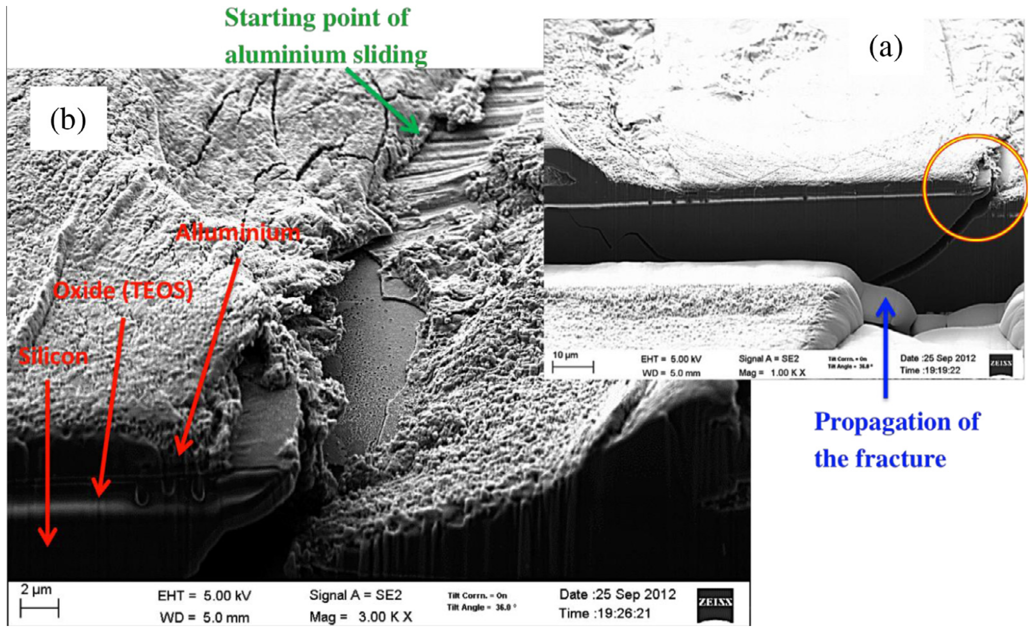

Fig. 6. Section of a bond tested in a non-destructive way showing a FM 0, where copper ball has been removed with acid in order to offer a completely visible pad: (a) magnification of the crack initiation site and (b) general view of the fracture surface. Fracture has been stopped at its beginning, so the starting point can be detected (crack has grown long according to the normal behaviour of a vitreous material; while aluminium has just started its sliding).

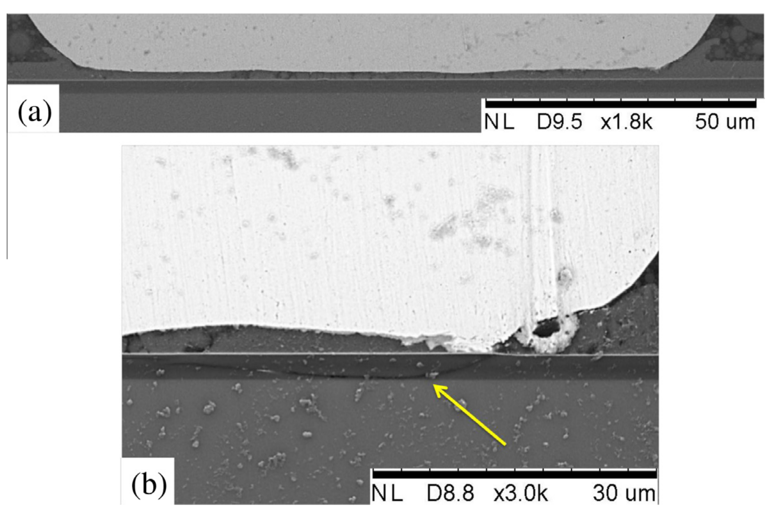

Fig. 7. Section of non-tested bond from the 2.0-mil-diameter batch (a) and the 2.5-mil-diameter batch (b). Aluminium pad of the 2.0 is non-over-deformed all along the bond interface. In some cases, the pad of 2.5 is so deformed that copper of the ball is in contact directly with the dielectric surface: ultrasonic power from the bonding process is directly applied on the silicon and can lead to the damage of the brittle material of the die because the damping buffer constituted by the aluminium is absent.

dielectric, meaning that the aluminium metal film has been locally squeezed-out: ultrasonic power from the bonding process is thus directly transferred to the underlying silicon oxide and silicon bulk, more susceptible of micro damaging due to their intrinsic brittleness and the local absence of the damping buffer constituted by the aluminium metal.

4. FEM modelling

Besides the experimental activities, fracture mechanics and the finite element method have been employed to model the pull and shear test with the aim to develop a numerical tool to predict the crack-path under the ball bond submitted to pull or shear test.

The general-purpose finite element program Abaqus [16] has been employed to build the models and carry out the simulations. In particular the analyses have been executed employing the implicit solver, as just static simulations have been performed. Fig. 8 shows the layout of the models and the load and boundary conditions which have been set. It is important to underline that the models must fulfil the requirements to reproduce as good as possible the experimental tests together with a high computational efficiency.

Since the pulling force has been thus assumed as applied vertically with respect to the die bond ball, as explained in the section concerning with the experimental work, the pull test is characterized by a complete axial-symmetry (geometry and load) and it has been modelled with a two-dimensional axial-symmetric model (see Fig. 8a).

The shear test, even though symmetrical by the point of view of geometry, is performed exercising pressure with a tool on a side of

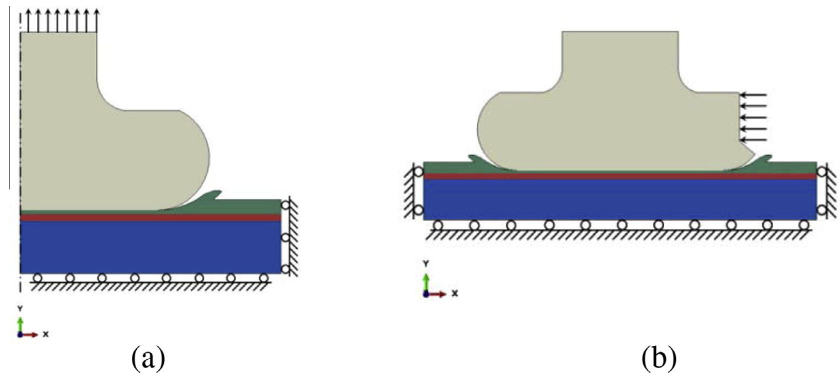

Fig. 8. Layout of the geometry and load and boundary conditions employed in the finite element models: (a) pull test and (b) shear test.

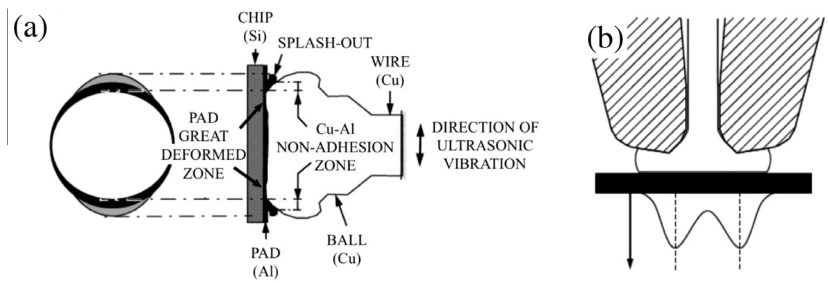

Fig. 9. Geometry [18] of the bond (a) and stress distribution [19,20] during wire bonding (b).

the ball-bond, which is not axial-symmetric loading condition. In this case a two-dimensional plane strain [17] model has been used (see Fig. 8b), which represents still a simplified approximation of the reality. However, even if the results must be carefully examined, they can provide at least a qualitative explanation of the crack initiation, i.e. in which direction it tilts, and extension.

Moreover, even if in the model geometrical details have been simplified, the bond geometry in all its significant aspects has been reproduced, e.g., in both the pull and the shear model the splash-out and pad great-deformed zone (see Fig. 9) have been carefully modelled in order to perfectly recreate the critical portion of the bond interface which represents the crack starter. The term splash-out [5] identifies the aluminium that protrudes at the sides of the wire ball, following to the pad deformation at the pad great-deformed zone. The bond geometry has been reproduced faithfully accordingly to bond measurements taken during the experimental campaign with the SEM. Furthermore, in the shear test model, the ball-bond deformation due to the pressure applied by the tool has been taken into account (see Fig. 8b).

In the pull test model, the load has been applied as a traction on top of the wire and the displacements have been restrained on the other two edges of the die (see Fig. 8a). In the shear test model, the load has been applied as a pressure to the ball in correspondence of the zone deformed by the tool, and the three edges of the die have been constrained as depicted in Fig. 8b. In particular, following to the experimental evidences (average values for the failure mode FM0 in Fig. 4), the load applied in the pull test simulations was 34.85 g, and 52.85 g in the simulations of the shear test.

The four different material layers can be distinguished in Fig. 8, whereas a better overview of the characteristics of the layers is given in Table 4: the main issue is that the chip bonding portion is composed by materials which have different elastic properties, thus leading to a deformation mismatch under loading conditions. This must be peculiarly critical at the interfaces between two contiguous layers and plays an important role in the extension of a potential crack. It is important to remark that each layer has been modelled accounting for its peculiar characteristics. Moreover, no interface has been modelled, so that the elements in two different layers share the same nodes.

Table 4
Characteristic of the modelled layers in terms of thickness and elastic properties of the materials.

Material	Colour	E (GPa)	ν	Thickness (μm)
Copper		130	0.36	(Ball)
Aluminium		73	0.334	1.53
Oxide		75	0.2	2.7 (dielectric)
Silicon		188	0.3	20

The aim of the finite element modelling has been to evaluate the stress intensity factors (SIF) in order to predict the crack path, which needs a proper mesh refinement in the region of the crack-tip. To this aim quadratic elements have been used, CAX8 for the axisymmetric model and CPE8 for the plane strain model [16] and the size of the elements around the crack tip has been set to 50 nm. Fig. 10 shows a magnification of the region in proximity of the crack tip in the first stage of crack extension, in which it is possible to observe that a number of 10 rings of extremely regular elements have been used at the crack tip in order to derive reliable values of the stress intensity factor, which is extremely important for a correct evaluation of the crack extension direction. Beyond the regular rings around the crack tip, a mesh coarsening has been adopted in order to reduce the number of elements, thus improving the computational efficiency. The size of the elements in the coarsened regions was not larger than 1.3 μm and an automatic algorithm has been used in order to prevent excessive element distortion, such as excessive aspect ratio.

In order to recreate the presence of a defect in the FEM model, the crack starting point has been set in correspondence of the beginning of the pad great-deformed zone and the initial crack

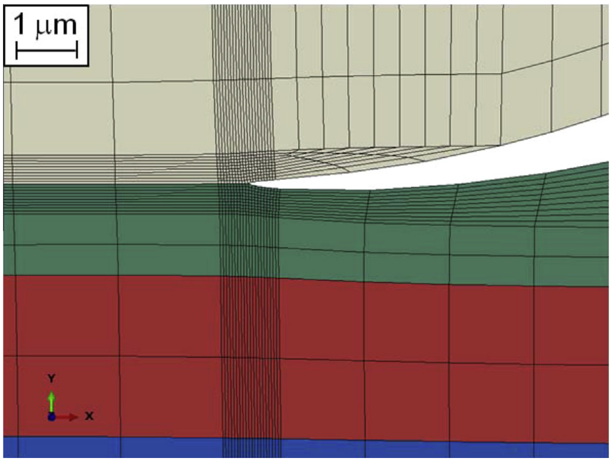

Fig. 10. Crack-tip modelling at the first stage of the crack extension.

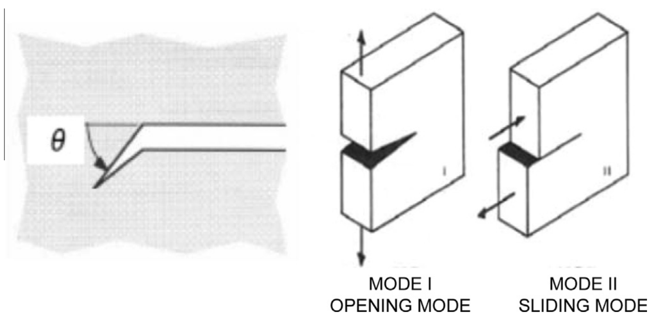

Fig. 11. Schematic of crack propagation in mixed mode [23].

has been modelled as an interface crack between copper and aluminium (see Fig. 10). Crack growth has been modelled through many consecutive steps: the FEM model does not account for automatic propagation of the crack from the starting point, therefore a stationary crack extension Δa has been modelled manually at each step to evaluate the SIF and the favourable angle for the crack propagation. Furthermore it must be underlined that a minimum of two crack extensions through each layer has been simulated in order to predict the crack path with enough accuracy. It is of some importance to remark that the less the crack extension (the more the steps), the better the predictions, especially when the crack approaches the interfaces. In this study the need for accuracy had to face the time-consuming modelling issues, as no automatic crack propagation algorithm has been employed. At the present stage, the time needed for the simulation of a single step of propagation on a usual personal computer is well within 10 s.

The second main issue of the numerical simulation, beside the calculation of the SIFs which is performed within Abaqus, is the calculation of the crack propagation angle [21,22], which has been performed according to a criterion for mixed-mode crack growth. There exist several criteria in the literature which are all energy or stress based [23,24]. In this work the maximum hoop stress criterion has been used as it represents a simple and widespread criterion for evaluating mixed-mode crack propagation. The fracture propagation direction θ can be found maximizing the hoop stress around the crack-tip:

$$\frac{\partial \sigma_\theta}{\partial \theta} = 0, \quad \frac{\partial^2 \sigma_\theta}{\partial \theta^2} < 0 \tag{3}$$

and taking into account the analytical stress distribution at the crack-tip expressed in polar coordinates [25] (see Fig. 11)

$$\sigma_\theta = \frac{1}{\sqrt{2\pi r}} \cdot \cos\left(\frac{\theta}{2}\right) \cdot \left[K_I \cos^2\left(\frac{\theta}{2}\right) - \frac{3}{2} K_{II} \sin(\theta)\right] \tag{4}$$

the direction of crack propagation θ_0 can be determined by substituting (4) in (3):

$$K_I \cdot \sin(\theta_0) + K_{II} \cdot [3 \cdot \cos(\theta_0) - 1] = 0 \tag{5}$$

It must be considered that this criterion has been adopted also for the initial stage of the propagation, when the crack lies in the interface between the aluminium and copper layer, even though it holds for homogeneous materials. In case of an interface crack, the crack-tip singularity field is characterized by a complex stress intensity factor $K = K_1 + iK_2$, in which K_1 and K_2 coincides with the standard mode I and II stress intensity factor only when the dissimilarities between the elastic properties of the two materials vanish [26]. Following this statement, the initial kinking angle calculated here must be taken only as an indication of the propagation direction, i.e., whether the crack kinks in the compliant or stiff material.

The working flow for the iterative calculations can be finally given as follows:

1. An initial crack is modelled by finite elements.
2. The SIFs are calculated.
3. The crack propagation direction for a new crack is determined by the foregoing relationships.
4. A new crack extension Δa in the new direction is modelled.

As a final modelling issue, it should be considered that intermetallic compounds (IMC) have not been modelled. The reason is that, taking into account the experimental campaign results, fracture has occurred starting from the aluminium and it propagated down to the silicon layer without involving the intermetallic layer. Moreover, the IMC layer thickness has been measured for each stress situation and the measurements showed no significant growth. Finally, no Kinrkendall void formation has been detected for any sample analysed.

However, being IMC the adhesion element between copper and aluminium, these are involved in the transmission of stresses between these two layers: this means they have a basic role on bond failure mechanisms [27] and in contributing defining the crack propagation even if they are not directly involved in the crack propagation path. For these reasons, although the geometry of the IMC coverage [28] has been studied, their effect on the stress intensity factor is not considered.

5. FEM results

An example of the early stage of crack propagation in the simulation of the pull test is depicted in Fig. 12. The first important consideration can be drawn regarding the crack propagation direction. If the material would be homogeneous, one would expect a propagation in pure mode I, i.e. on a plane perpendicular to the loading direction, as the starting crack plane lies perpendicular to the loading direction. In the problem here investigated, the dissimilarity between the elastic properties of the two layers is of great influence on the predicted direction, which gives rise to a considerably high mode II and promotes a crack deviation from a straight path and the crack kinks in the more compliant material.

These results confirm the findings by He and Hutchinson [26], even though they must be carefully interpreted due to the complex nature of the stress intensity factors in an interface crack problem. In particular, they found that the interface crack kinks in the more

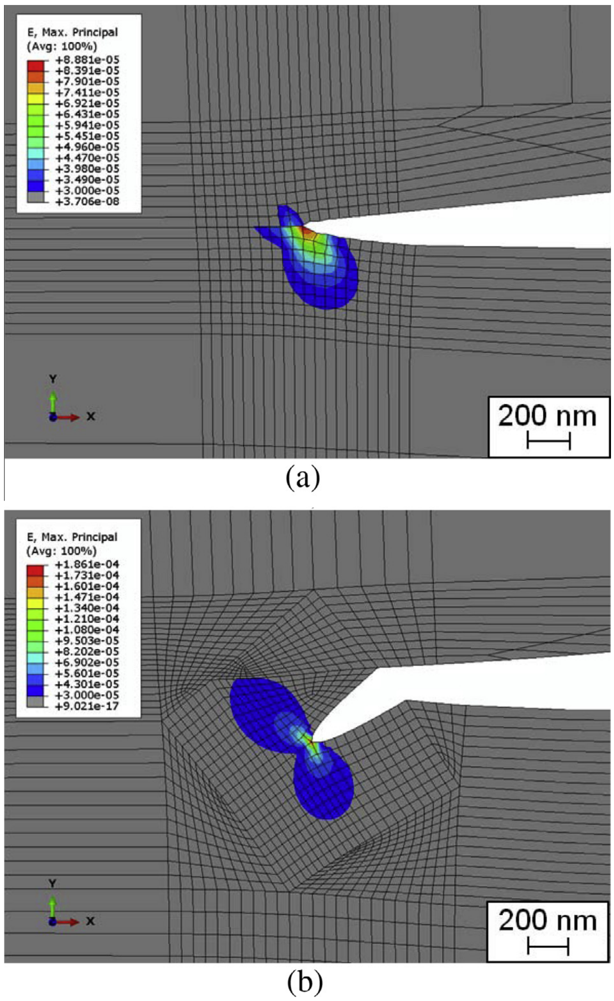

Fig. 12. Maximum principal strain in the early stage of crack propagation in the pull test: (a) initial iteration and (b) second iteration.

compliant material even if the loading direction is perpendicular to the crack plane. It must be underlined that, according to [26], the dissimilarity in the elastic properties is a necessary condition to understand whether the crack will kink out of the interface, but it is not sufficient. In fact a relevant role is played also by the ratio between the toughness of the more compliant material and the interface. If the toughness of the more compliant material is sufficiently higher than the one of the interface, then the crack will never kink out and it will propagate further in the interface. In the present research no data about the toughness of the interface were available, but the experimental evidences showed the cracks kinking out of the interface to propagate into the more compliant material.He and Hutchinson based their work on special parameters, α and β, which have been introduced by Dundurs [29] in the discussion of the original paper by Bogy [30] on the singular stress field at the interface of dissimilar orthogonal elastic wedges subjected to normal and shear loading. These two parameters are really useful in the description of the stress field across the interface and, therefore, also to work out the dependency of the energy release rate for crack propagation on the elastic properties of the dissimilar elastic materials.

Considering a stiff material 1 (copper) and a compliant material 2 (aluminium), under the hypothesis of plane-strain, it is possible to define the Dundurs parameters as follows [21,22]:

$$\alpha = [G_1 \cdot (1 - \nu_2) - G_2 \cdot (1 - \nu_1)]/[G_1 \cdot (1 - \nu_2) + G_2 \cdot (1 - \nu_1)] \quad (6)$$

$$\beta = \frac{1}{2} \cdot [G_1 \cdot (1 - 2 \cdot \nu_2) - G_2 \cdot (1 - 2 \cdot \nu_1)]/[G_1 \cdot (1 - \nu_2) + G_2 \cdot (1 - \nu_1)] \quad (7)$$

where $G = E/[2 \cdot (1 + \nu)]$ and ν are the shear modulus and the Poisson's ratio respectively. For an interface crack between copper and aluminium (which is the case of the present study) $\alpha = 0.29$ and $\beta = 0.08$ which predicts the crack kinking into the aluminium layer (more compliant material) according to He and Hutchinson [26]. Furthermore it has to be noted that the system Cu/Al is characterised by a very low value of the parameter β as it is the case for

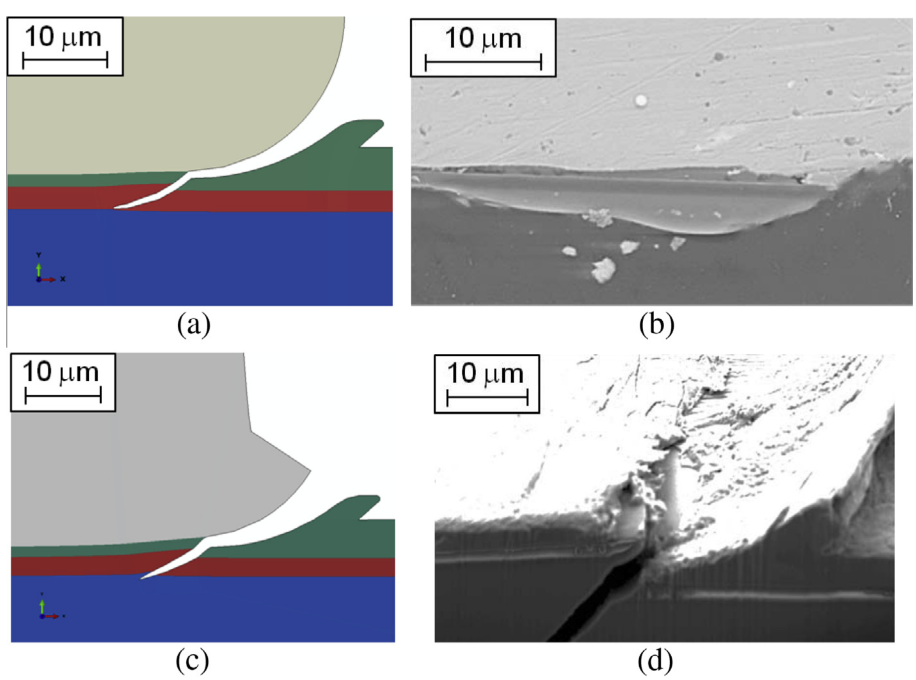

Fig. 13. Comparison between the numerical predicted and the experimental crack path in the tests: (a) simulation of the pull test; (b) experimental pull test; (c) simulation of the shear test and (d) experimental shear test.

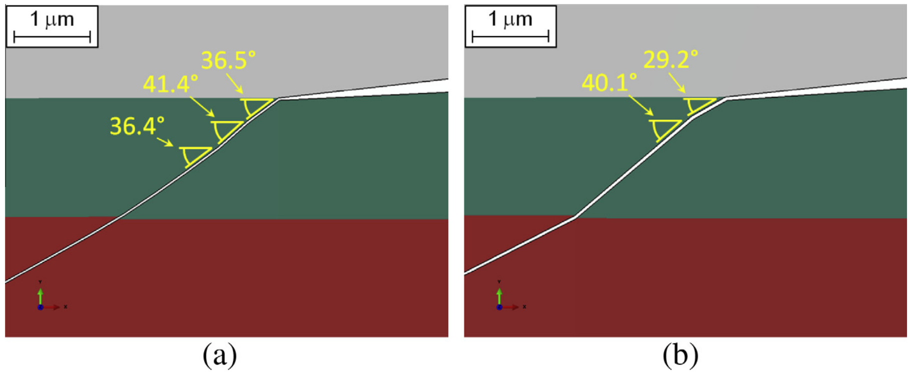

Fig. 14. Comparison between the numerical predicted kink angle: (a) pull test and (b) shear test.

Table 5
Comparison between experimental and FEM results.

Test method	ΔF (%)	Acceptable failure mode SIF	Not acceptable failure mode SIF	ΔSIF (%)
Pull	69	2.639	4.682	77
Shear	0.04	72.43	71.76	1

many other pairs of materials which can be found in the literature [22,26].

The dissimilarity in the elastic properties can be appreciated also by the contours of the maximum principal strain depicted in Fig. 12a, in which the greater deformation occurs in the aluminium layer. When the crack is full immersed in the homogeneous material, the deformation becomes symmetrical respect to the crack plane and the crack tends to propagate straight (see Fig. 12b).

Comparing the crack path predicted by the numerical model with the one obtained in the experiments, both the pull test model and the shear test model can be said to be reliable as they yield a good predictions (see Fig. 13). In particular, in the simulation of the pull test, as the crack approaches the interface between the aluminium and oxide, it tends to grow through the interface, as the two materials have similar properties. When the crack approaches the interface between oxide and silicon, it kinks in order to propagate in the more compliant material further, which has been also observed experimentally (see Fig. 13b). On the contrary, the simulation of the shear test (see Fig. 13c) predicts a crack growing through the interface between oxide and silicon, which reproduces correctly the experimental evidences shown in Fig. 13d. Further calculations of the kink angle for the interface crack are depicted in Fig. 14. Despite the different loading conditions (pull and shear), the interface cracks grow in the same direction through the layer of aluminium.

Moreover, comparing the difference in mechanical strength (ΔF) between acceptable and not acceptable failure modes, which represents the bond deterioration rate, (in other words, the gap between patterns relative to acceptable and not acceptable failure modes of Fig. 4a and b) with the difference between the stress intensity factor (ΔSIF) evaluated for an acceptable and a not acceptable failure mode (see Table 5) it can be said that the numerical model gives an excellent qualitative prediction of the failure mode. As it has been the case for ΔF in the experimental tests, also in the case of numerical simulations ΔSIF between acceptable and not acceptable modes is an indicator of which failure mode occurred. The higher the gap (ΔSIF), the clearer the evidence of a not acceptable failure mode. The fact that the larger ΔSIF has been obtained for the pull test speaks in favour of using this test mode, rather than the shear test, as indicator of not acceptable failures.

It is of some importance to remark that the present state of the research does not give the possibility to provide predictions which are also quantitatively good. If it is true that the simple models are able to reproduce the crack paths observed in the tests, some modelling assumptions must be proved further, which implies the use of 3D models, the modelling of the interface behaviour and in the last instance the adoption of an automatic propagation algorithm. Having said that, the current models could be used in the early stage of pad design in order to prevent failures. In particular a sentivity analysis could be performed in order to investigate the influence of different elastic properties on the propagation angle. Other parameters to be investigated could be the thickness of the layers and the optimum geometry of the interface between ball and pad. Another interesting investigation could be performed about the influence of different fracture toughness properties of the materials and the interfaces, in order to predict whether the crack grows through the layers or through the interfaces.

6. Conclusion

Wire pull and ball shear test are consolidated practices for quality and reliability assessment of gold wire-bonds. Their extension in the field of copper wire, due to the higher stiffness of this material, requires a deeper study of the crack propagation mechanisms in the bond-pad structure, in order to establish a correct set of acceptance criteria able to separate the intrinsic failure modalities from possible weaknesses induced by inappropriate bonding.

The combined use of bond cross-sectioning after non-destructive pull / shear testing and FEM modelling provides an effective tool for the experimental characterization and advanced prediction of the crack propagation modalities.

The present work has identified wire pull test as best method for the detection of mechanically-weak joints between copper wire and aluminium bond-pads, as the breaking load distributions of the "normal" and "potentially-critical" failure modes exhibit a more significant shift than those obtained from ball shear test.

The FEM model developed has provided a good correlation between the experimental and simulated crack path through the usage of SIF, which can be effectively applied to predict the expected failure modes during pull or shear tests depending on the bond-pad structure design and the ball bond morphological features. Therefore, it would be highly helpful to silicon process designers and wire-bonding engineers in the difficult task of optimizing the compatibility between bond-pad structure and ball-bonding parameters for a reliable component performance.

Pioneering objectives like designing active circuits and metal routing under the thick copper bond, and modelling the acceleration factors related to reliability stress in presence of damages or cracks, represent key areas of potential application for the SIF-based FEM simulations.

Acknowledgments

This work has been developed within a research agreement between Politecnico di Milano and ST-Microelectronics and has been supported by the ST-Microelectronic R&D laboratories of Agrate and Cornaredo Italian sites.

The authors would like to thank Prof. Teresa Ting for advice and support.

References

[1] Kim HJ, Lee JY, Paik KW, Koh KW, Won J, Choe S, et al. Effects of Cu/Al intermetallic compound (IMC) on copper wire and aluminum pad bondability. IEEE Trans Comp Package Technol 2003;26(2):367–74.
[2] Nishimura A, Kawai S, Murakami G. Effect of lead frame material on plastic-encapsuled IC package cracking under temperature cycling, electronic components conference, Huston, TX, May 22–24, 1989, proceedings, 39th. IEEE Trans Comp Hybrids Manuf Technol December 1989;12(4).
[3] Vitali B, Frontero A. Capillary for bonding copper wires between a semiconductor circuit chip and a corresponding terminal connector of a semiconductor device. U.S. Patent 6 581 816 (B2) in the name of STMicroelectronics S.r.l. June 24; 2003.
[4] Hang CJ, Song WH, Lum I, Mayer M, Zhou Y, Wang CQ, et al. Effect of electronic flame off parameters on copper bonding wire: Free-air ball deformability, heat affected zone length, heat affected zone breaking force. Microelectron Eng, Elsevier 2009;86(10):2094–103.
[5] Pecht MG, Zhong A, Choubey A, Chauan PS. Copper wire bonding. Springer; 2014, ISBN 978-1-4614-5761-9.
[6] Harman GG, Cannon CA. The microelectronic wire bond pull test – how to use it, how to abuse it. Paper presented as a part of the semiconductor technology program at the national bureau of standards, at the 28th electronic components confederence, Anaheim, CA, April 24–26, 1978. IEEE transaction on components, hybrids, and manufacturing technology, vol. 1(3); 1978, p. 203–10.
[7] Harman G. Wire bonding in microelectronics: materials, processes, reliability and yield. New York: McGraw-Hill; 1997. ISBN-13: 978–0070326194.
[8] Wei TC, Daud AR. Cratering on thermosonic copper wire ball bonding. J Mater Eng Perform June 2002;11(2):283–7.
[9] Hellen TK, Blackburn WS. The calculation of stress intensity factors for combined tensile and shear loading. Int J Fract 1975;11(4):605–17.
[10] Dunn CF, Mcpherson JW. Temperature-cycling acceleration factors for aluminium metallization failure in VLSI applications. In: Reliability physics symposium, 28th annual proceedings, international; 1990, p. 252–58.
[11] Tobias PA, Trindade DC. Applied reliability. 2nd ed. Van Nostrand Reinhold Company; 1995. ISBN-13: 978–1584884668.
[12] Standard Test Method for Measuring Pull Strength of Microelectronic Wire Bonds. ASTM standard test method: F459-06. Annual listing of ASTM standards. ASTM International West Conshohocken, Pennsylvania, USA; 2006.
[13] Standard Non-Destructive Pull Testing of Wire Bonds. ASTM standard test method: F458-06. Annual listing of ASTM standards. ASTM International West Conshohocken, Pennsylvania, USA; 2006.
[14] Test Method for Destructive Shear of Ball Bonds. ASTM standard test method: F1269-06. Annual listing of ASTM standards. ASTM International West Conshohocken, Pennsylvania, USA; 2006.
[15] Charles Jr. HK, Clatterbaugh GV, Weiner JA. The ball bond shear test: its methodology and application. In: Semiconductor Processing, STP 850, Gupta D.C. (Ed.), American Sociaty for Testing and Materials; 1984, p. 429–31.
[16] Abaqus 6.12-1. User's Manual, Dassault Systemes Simulia Corp.
[17] Gere JM, Timoshenko SP. Mechanics of materials. 3rd SI ed.. London: Chapman and Hall; 1991.
[18] Shah A, Rezvani A, Mayer M, Zhou Y, Persic J, Moon JT. Reduction of ultrasonic pad stress and aluminium splash in copper ball bonding. Microelectronics reliability, Elsevier 2011;51(1):67–74.
[19] Hang CJ, Wang CQ, Mayer M, Tian YH, Zhou Y, Wang HH. Growth behaviour of Cu/Al intermetallic compounds and cracks in copper ball bonds during isothermal aging. Microelectronics reliability, Elsevier 2008;48(3):416–24.
[20] Anand TJS, Yau CK, Huat LB. Oxidation study on as-bonded intermetallic of copper wire-aluminium bond pad metallization for electronic microchip. Mater Chem Phys 2012;136(2–3):638–47.
[21] Hutchinson JW, Suo Z. Mixed mode cracking in layered materials. Advances in Applied Mechanics 1992;29:63-75–126-30.
[22] Hutchinson JW, Mear ME, Rice JR. Crack paralleling an interface between dissimilar materials. J Appl Mech December 1987;109:828–32.
[23] Pook LP. Crack paths. WIT Press; 2002. ISBN 1-85312-927-5.
[24] Sweldow JL. Criteria for growth of the angled crack. Cracks and fractures, ASTM STP 601. Philadelphia, PA: American Society of Testing and Materials; 1976, p. 506–21.
[25] Beretta S, Desimone H, Madia M, Poli A. Multiaxial fatigue and defect assessment of truck stabilizers. Int J Vehicle Des 2006;40(1–3):212–27.
[26] He M-Y, Hutchinson JW. Kinking of a crack out of an interface. J Appl Mech 1989;111.
[27] Clatterbaugh GV, Charles Jr. HK. The effect of high-temperature intermetallic growth on ball shear-induced cratering. Electronic components conference, Huston, TX, May 22–24, 1989. In: Proceedings, 39th, IEEE transactions on components. Hybrids and manufacturing technology, vol. 13(1); 1990.
[28] Wulff FW, Breach CD, Stephan Saraswati D, Dittmer KJ. Characterization of intermetallic growth in copper and gold ball bonds on aluminium metallization. In: IEEE conference publications, electronics packaging technology conference, proceedings of 6th EPTC; 2004, p. 348–53.
[29] Dundurs J. Discussion: edge-bonded dissimilar orthogonal elastic wedges under normal and shear loading (Bogy DB. ASME J Appl Mech, vol. 35, 1968, p. 460–66). J Appl Mech September 1969;36(3):650–2.
[30] Bogy DB. Edge-bonded dissimilar orthogonal elastic wedges under normal and shear loading. J Appl Mech September 1968;35(3):460–6.